

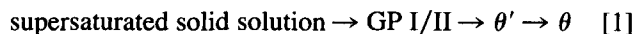
A Calorimetric Study of Precipitation in an Al-Cu Alloy with Silicon Particles

M.J. STARINK and P. VAN MOURIK

The precipitation of copper and silicon from the Al-rich matrix in an Al-1.3 at. pct Cu-19.1 at. pct Si alloy was investigated by differential scanning calorimetry (DSC). Both as-extruded (AE) and extruded and solution treated and quenched (solid-quenched, SQ) specimens were studied. The DSC curves of the SQ specimens showed two exothermic effects, A and B. Effect A corresponded to the simultaneous precipitation of silicon and copper, whereas effect B was caused by the transition from the state with the intermediate copper-containing phase, θ' , to the state with the equilibrium copper-containing phase, θ . The heat contents of effect A and B could quantitatively be described in terms of solid solubilities before and after precipitation and the heats of precipitation of the phases involved. From this description, it was derived that for heating rates ≤ 20 K/min, copper precipitated as the θ' phase, while for heating rates ≥ 40 K/min, copper precipitated mainly as the θ phase. In SQ specimens, Guinier-Preston (GP)-zone formation occurred during aging at room temperature with a rate approximately 10^4 times slower than in the corresponding binary Al-Cu alloy. For the AE specimens, it was found that during extrusion, precipitation of copper and silicon proceeded to a large extent. However, from DSC experiments and from hardness measurements as a function of aging time at 453 K, it was deduced that copper precipitation had not finished during extrusion. The hardness increase as observed during aging directly after extrusion was interpreted to be due to formation of the semicoherent intermediate θ' phase.

I. INTRODUCTION

IN quenched binary Al-Si alloys, precipitation directly results in the formation of the equilibrium phase,^[1] whereas in quenched Al-Cu alloys, precipitation proceeds *via* intermediate phases according to a temperature-dependent sequence. At sufficiently low temperatures, the following scheme applies:^[2]



where GP I/II stands for Guinier-Preston zones,* θ' is

*Until recent publications, discussion about the nature of GP I/II zones has persisted.^[3] Guinier-Preston II zones are considered to be a slightly modified (multilayered) form of (predominantly monolayered) GP I zones or to be a different phase (then the term θ'' phase, instead of GP II zones, is usually preferred). In this paper, the term GP I/II is used. In any case, GP II is subsequent to GP I.

a transition phase having a structure which is a tetragonal distortion of the CaF_2 structure and which has a composition Al_2Cu , and θ is the equilibrium phase having a body-centered tetragonal structure with the same chemical composition as θ' .^[2]

The equilibrium solid solubility of both alloying elements (Si and Cu) decreases with decreasing temperature, and the aluminum-rich corner of the Al-Cu-Si system does not show any intermediate ternary phase.^[4] Hence, on aging of a quenched Al-Cu-Si alloy, precipitation of the phases occurring in the constituting binary systems will take place. To our knowledge, no explicit

studies on the precipitation phenomena in quenched Al-Cu-Si alloys have been reported until now.

In view of potential applications, the optimization of the mechanical properties and heat treatments (if required) of metal-matrix composites (MMCs) is important. Several studies were devoted to the heat treatment of MMCs.^[5-10] It was generally found that the aging response of MMCs was faster than of the corresponding alloy without reinforcement.

Melt spinning of Al-Cu-Si alloys with amounts of silicon beyond the maximal solid solubility for silicon yields finely grained ribbons with finely, homogeneously dispersed silicon particles.^[11] After hot extrusion, the silicon size distribution is comparable to the particle size distribution in MMCs.^[11] Further, as the Al-Cu-Si alloy combines the presence of a heat-treatable Al-matrix with the presence of silicon particles, this alloy can be considered as a model for studying precipitation phenomena in particle-reinforced MMCs. On temperature changes, the presence of silicon particles embedded in an Al-rich matrix introduces a large volume misfit between matrix and reinforcing particles (also characteristic for most MMCs) because of the large difference in coefficients of thermal expansion of the Al-rich matrix and silicon ($23.5 \times 10^{-6} \text{ K}^{-1}$ and $3 \times 10^{-6} \text{ K}^{-1}$, respectively; see Reference 12). From a comparative study on heat effects in an Al-Cu alloy with and without silicon particles, it appeared that in the Al-Cu alloy with silicon particles, GP-zone formation was effectively hindered, whereas the main precipitation of θ'/θ phases was enhanced.^[13] Corresponding changes in precipitation kinetics were observed in several solid-quenched MMCs.^[6,7,8]

Because extruded MMCs may be used after a complete heat treatment (solid solution homogenizing, solid quenching plus aging) as well as directly after extrusion,

M.J. STARINK, Graduate Student, and P. VAN MOURIK, Scientist, are with the Laboratory of Metallurgy, Delft University of Technology, Rotterdamseweg 137, 2628 AL Delft, The Netherlands.

Manuscript submitted January 29, 1990.

knowledge of precipitation both after solid quenching and after extrusion is desirable. Therefore, it was decided to study the precipitation in a melt-spun Al-Cu-Si alloy both after homogenization and solid quenching and after extrusion. As both silicon and copper precipitation from an Al-rich matrix are associated with enthalpy changes that are large enough to allow differential scanning calorimetry (DSC),^[1,14] the precipitation study was performed by this technique. In addition, hardness measurements were performed.

II. EXPERIMENTAL PROCEDURES

Liquid-quenched Al-1.3 at. pct Cu-19.1 at. pct Si ribbons were produced by melt spinning from 99.998 wt pct Al, 99.99 wt pct Si, and 99.9 wt pct Cu. The melt-spinning process was described earlier.^[15] Typical dimensions of the ribbons obtained were: thickness, 50 μm , and width, 3 mm. The ribbons were chopped into flakes with a length ranging from 1 to 5 mm. The flakes were dried up to 24 hours at a temperature of 380 K to eliminate possibly attached moisture. Subsequently, the flakes were precompact to cylindrical billets with a density of about 65 pct of the maximal density. Prior to extrusion, the billets were preheated at the extrusion temperature of 650 K for 20 minutes. Extrusion took place at a reduction ratio of 20:1. A bar with a diameter of 11 mm, of which a large part showed a density of 100 pct, was produced. After extrusion, the bar was cooled in air. For practical reasons, the air cooling was completed after 10 minutes by a water quench.

From the part of the bar with a density of 100 pct, thin (thickness about 1 mm) specimens were cut for investigation. Differential scanning calorimetry was performed in the as-extruded (AE) condition and in the as-extruded and subsequently aged (AE + A) condition. Aging took place at 453 ± 2 K. Besides, specimens were homogenized at 793 ± 2 K and subsequently quenched into water. Differential scanning calorimetry experiments were conducted 1 hour after this solid quenching (SQ specimens) or took place as a function of time of natural aging, *i.e.*, at room temperature [SQ + NA (natural aged) specimens]. In Figure 1, a schematic representation of temperature as a function of time during the production of an AE and/or SQ specimen is given.

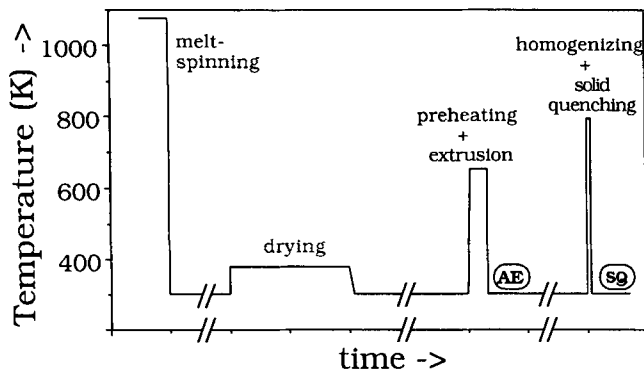


Fig. 1—Schematic representation of temperature as a function of time during the production of AE and/or SQ specimens.

The DSC apparatus used was a Dupont type 910. Calibration runs were carried out with pure indium, zinc, tin, and lead. Calibration of both the temperature and heat effect scales was obtained using the known^[16] melting points and heats of melting of these metals. The heat effect scale was calibrated at all heating rates employed. As a reference, pure aluminum (99.99 pct) with a mass close to that of the specimen was used. Both reference and specimen were enclosed in an aluminum pan sealed with an aluminum cover. A protective gas atmosphere of pure argon was employed. For the SQ specimens, the following DSC heating rates were applied: 0.5, 2, 5, 20, 40, and 80 K/min; for the other specimens, only 20 K/min was applied. Runs were recorded between 300 and 791 K. As beyond 740 K only heat effects corresponding to dissolution were observed in the DSC curves, in this precipitation study only the temperature interval 300 to 740 K will be considered. After the first run, the specimen was maintained at 791 K for 2 minutes; subsequently, it was allowed to cool freely inside the DSC apparatus for 200 minutes. The cooling of all specimens after the first run was identical and nearly exponential; the cooling rate on passing the copper solvus at 750 K^[4] was 22 K/min, and on passing 550 K, the cooling rate was 6.5 K/min. At the end of the cooling, room temperature was reached. Subsequently, a second run, at the same heating rate as the first run, was performed. The DSC curves presented were generally obtained by subtracting the baseline from the first run. The slight differences in heat capacity between the specimen before and after precipitation were ignored. This is justified in view of the fact that all of the measured heat capacities of the specimens investigated correspond to the predictions based on the Kopp and Neumann rule.^[17]

Microhardness of the AE + A specimens was measured on longitudinal sections through the axis of the extruded bar using a LEITZ DURIMET* Vickers hard-

*LEITZ DURIMET is a trademark of Leitz, Inc., Rockleigh, NJ.

ness tester. For each hardness value, at least 10 indentations evenly distributed over a line from the axis to the edge of the bar were made (hardness did not depend on the radial distance to the center of the bar).

III. RESULTS

Both after extrusion and after solid quenching, a homogeneous dispersion of silicon particles was observed both in transverse and longitudinal sections (*cf.* Figures 2 and 3). The average silicon particle size after extrusion was about 0.5 to 1 μm (Figure 2). After subsequent homogenizing and quenching, the silicon particle size had increased to about 1 to 2 μm (Figure 3). Typical examples of a first and a second run DSC curve for an SQ specimen are shown in Figure 4(a). From Figure 4(a), it follows that during the second run, no exothermic heat flow occurs. This is interpreted as such that, during cooling after the first run, precipitation proceeds completely. Thus, the curve obtained by subtracting the second run from the first run reflects only the difference in free enthalpy just before the runs

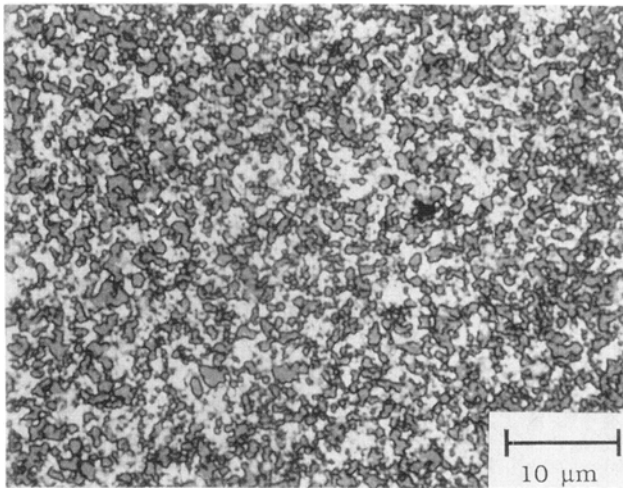


Fig. 2—Transverse section of the AE Al-1.3 at. pct Cu-19.1 at. pct Si alloy; optical micrograph.

(Section II). The DSC curves to be presented in this study are always such rerun-corrected curves.

At sufficiently low heating rates, the sequence 1 (Section I) for precipitation in quenched Al-Cu alloys is generally revealed by DSC studies,* confirmed by elec-

*As precipitation reactions are usually controlled by diffusion, an increase of the DSC heating rate results in an increase of the precipitation temperatures. This has a twofold effect: (1) the amount of precipitating atoms decreases due to the increased solid solubilities at the increased precipitation temperatures, and (2) the share of phases stable at high temperatures in the total amount of precipitating phases increases. In the case of Al-Cu alloys, it can be expected that at sufficiently high heating rates, all copper precipitation involves the stable θ phase (Sections IV-A-1 and IV-A-2).

tron microscopy,^[18] and corroborated by hardness measurements.^[14] Thus, such a DSC curve displays exothermic effects: GP-zone formation, θ'/θ precipitation and transformation of a state with θ' phase to a state with θ phase, and endothermic effects: GP-zone dissolution, θ' -phase dissolution, and θ -phase dissolution (both given in the order from low to high temperature). For SQ Al-Si

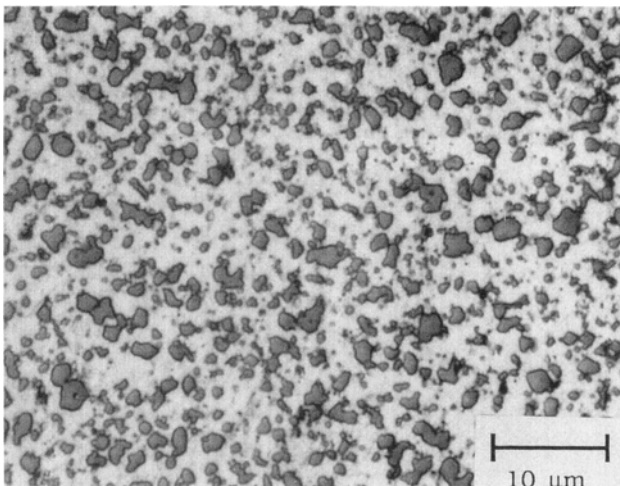
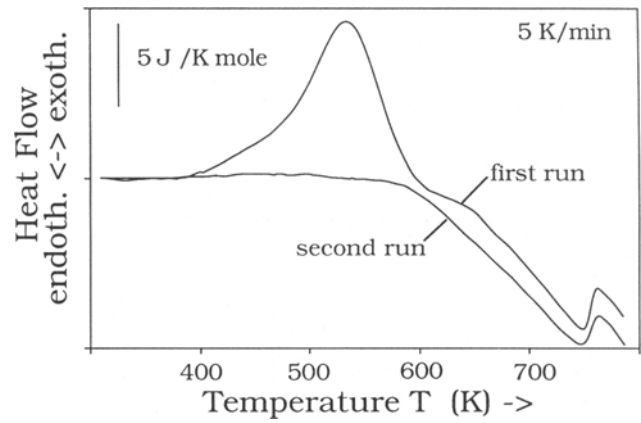
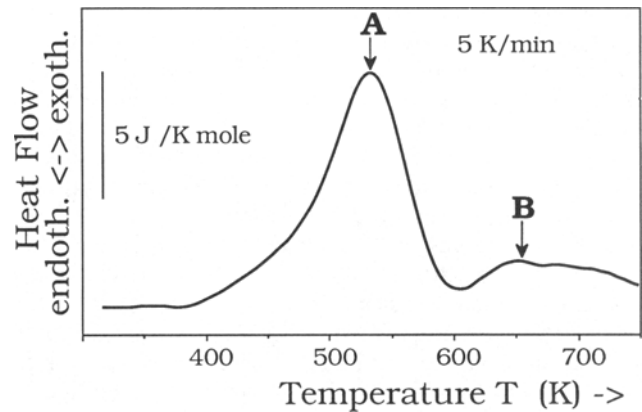


Fig. 3—Longitudinal section of the SQ Al-1.3 at. pct Cu-19.1 at. pct Si alloy; optical micrograph.



(a)



(b)

Fig. 4—(a) DSC curves of the first and the second run of the SQ Al-1.3 at. pct Cu-19.1 at. pct Si specimen (heating rate is indicated). (b) Rerun-corrected DSC curve of the SQ Al-1.3 at. pct Cu-19.1 at. pct Si specimen (heating rate is indicated).

alloys, the effects in DSC curves cannot be misinterpreted, as only one exothermic and one endothermic effect occurs.^[1] The observed effects beyond 740 K were interpreted before as due to the last stages of copper dissolution and a continuing silicon dissolution.^[13] Hence, the starting temperatures of these effects are independent of the DSC heating rate, as was observed.

A typical example of a rerun-corrected curve for an SQ specimen is given in Figure 4(b), in which two effects, A and B, can be discerned. As the free enthalpy of the specimen just before the first run is higher than before the second run (the matrix of the SQ specimen is supersaturated), the effects to be observed in the rerun-corrected curve will generally be exothermic. Based upon the foregoing (see previous paragraph), the exothermic effects A and B in Figure 4(b) are interpreted as follows. Effect A is the simultaneous precipitation of silicon and θ or θ' phase. Effect B is the transformation from a state with θ' -phase precipitates to a state with θ -phase precipitates. As the DSC heating rate was increased, the effects were observed to shift to higher temperatures, implying an increase of the peak and end temperatures of effect A.

All heat contents presented were determined by measuring the area between the rerun-corrected DSC curve and a straight line obtained by connecting points on the DSC curves at 350 and 740 K. At low heating rates, the effects A and B were observed separately, whereas at heating rates of 40 and 80 K/min, overlap of effects A and B occurred. In these cases, the respective heat contents were obtained by a correction based on an extrapolation of the heat flow of effect A at temperatures where effects A and B coexisted. The effect B did not show a well-defined peak temperature as effect A did; at the heating rates of 20 and 40 K/min, two maxima could be discerned for effect B. In Table I, the peak and end temperatures of effect A and the heat contents of effects A and B are gathered. It is observed that the heat contents of effects A and B decrease with increasing DSC heating rate.

The heat contents of effects A and B as observed for the SQ + NA specimens did not depend on the times of natural aging applied. However, after natural aging, a small endothermic effect was observed just in advance of effect A (Figure 5). This endothermic effect is thought to be caused by the dissolution of GP zones (Section IV-A-3). The heat content of this effect increases with increasing time of natural aging (Figure 6).

The DSC curves taken after extrusion (AE) and after aging (AE + A) for 4, 28, and 192 hours at 453 K did not show pronounced peaks that could be related to some precipitation reaction; *i.e.*, the first DSC run and the rerun showed a strong resemblance. Nevertheless, the rerun-corrected DSC curves resulting from the subtraction of the rerun scans from the first run scans indicate (Figure 7) the following:

- (1) the heat flows observed above 675 K for the AE and AE + A specimens are equal within the experimental error, indicating corresponding end states;
- (2) for the AE specimen, a small exothermic effect is observed between about 350 and 600 K; no such effect is observed for the AE + A specimens; and
- (3) for the AE + A specimens, an endothermic effect is observed between about 500 and 650 K; the magnitude of this effect increases with increasing aging time.

The AE specimens show a marked response to aging: Figure 8 shows the hardness as a function of the time of aging at 453 K. It is observed that 0.5 hours aging sig-

Table I. Peak and End Temperatures of Effect A and Heat Content of Effects A and B in Solid-Quenched Al-1.3 At. Pct Cu-19.1 At. Pct Si as a Function of Differential Scanning Calorimetry Heating Rate

Heating Rate (K/min)	Peak Temp. of Effect A (K) ± 3 K	End Temp. of Effect A (K) ± 5 K	Heat Content of Effect (J per Mole Alloy)	
			A	B
0.5	488	525	770 \pm 40	80 \pm 30
2	514	570	730 \pm 30	60 \pm 20
5	538	595	710 \pm 30	60 \pm 20
20	567	640	610 \pm 30	41 \pm 11
40	600	675	640 \pm 20	12 \pm 5
80	617	705	580 \pm 30	8 \pm 5

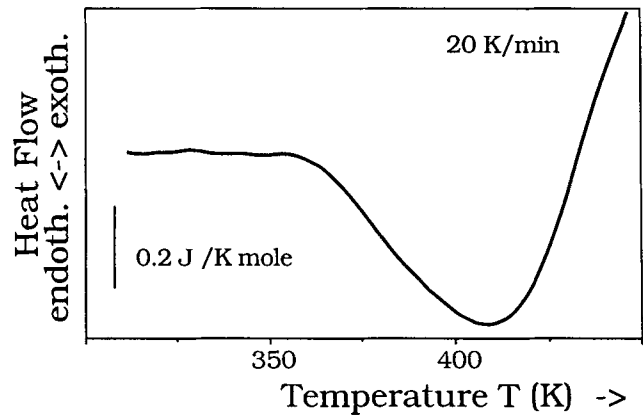


Fig. 5—First part of the rerun-corrected DSC curve of the SQ Al-1.3 at. pct Cu-19.1 at. pct Si specimen aged for 1032 h at room temperature. Note the scale difference with Fig. 4 (heating rate is indicated).

nificantly increases the hardness of the AE specimens. Maximum hardness is reached after about 30 hours of aging, followed by overaging (hardness decrease).

IV. DISCUSSION

A. Precipitation Phenomena Observed for SQ Specimens

1. Effect A

It is thought that effect A can be understood as a result of the precipitation of the phases as occurring in the constituting binary alloys (Section III). The solid solubility of silicon in the precipitated θ (Al_2Cu) phase, as well as the solid solubilities of copper and aluminum in the silicon phase, is negligible.^[19] As can be deduced from the aluminum-rich corner of the Al-Cu-Si phase diagram,^[4] the solid solubility of either alloying element below the homogenizing temperature applied is not influenced by the presence of the other alloying element in solid solution. In view of the low solid solubilities concerned, it can be assumed that the heat effect of precipitation/dissolution of one element also is not influenced by the presence of the other element. Thus, it is reasonable to assume that the total heat of precipitation for the ternary

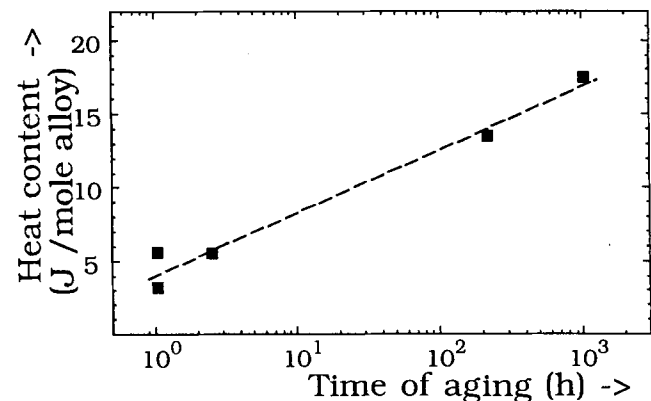


Fig. 6—Heat content of the endothermic effect preceding effect A as a function of the time of natural aging.

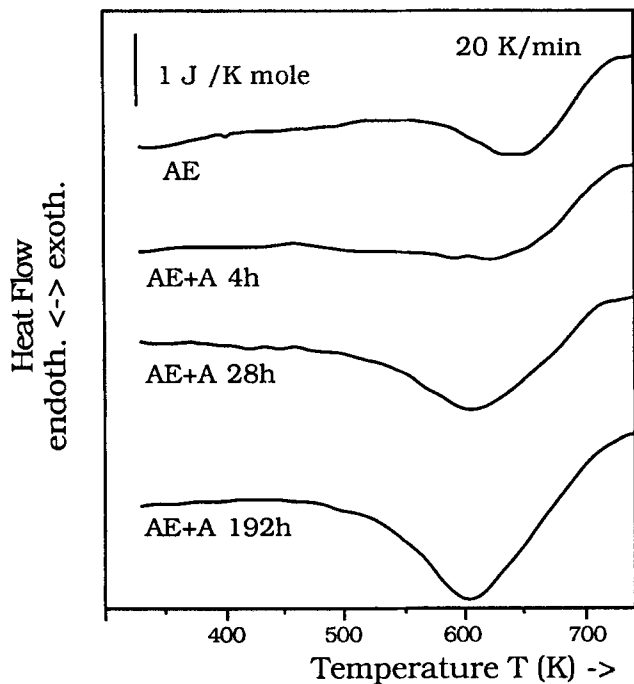


Fig. 7—Rerun-corrected DSC curves of the AE and the AE + A Al-1.3 at. pct Cu-19.1 at. pct Si specimens. For the AE + A specimens, the time of aging at 453 K is indicated. For reasons of clarity, the zero points of the curves were separated.

alloy is the sum of the heats of precipitation for the constituting binary aluminum alloys. The theoretical calculation of the total heat content of effect A based on these assumptions is outlined in Appendices I and II. To perform the calculation outlined in Appendix I, values for the mole fractions of copper and silicon dissolved in the Al-rich matrix before and after precipitation, x_{Cu}^0 , x_{Si}^0 and x'_{Cu} , x'_{Si} , respectively, are necessary (Eqs. [A12] and [A13]). The value for x_{Si}^0 (1.05×10^{-2}) was taken equal to the mole fraction of silicon dissolved at the homogenizing temperature.^[4] The value of x_{Cu}^0 (1.6×10^{-2}) was calculated according to Eq. [A2] (Appendix I), assuming complete dissolution of copper in the Al-rich matrix after solid quenching. It is noted that the equilibrium solid solubility of copper in the Al-rich matrix of the Al-Cu-Si alloy at the homogenizing temperature is

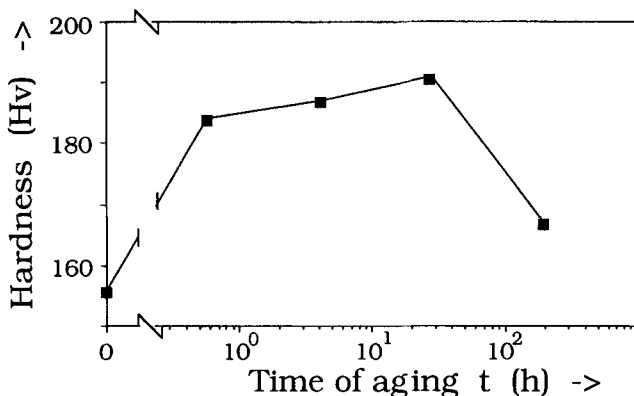


Fig. 8—Hardness of the AE and the AE + A Al-1.3 at. pct Cu-19.1 at. pct Si specimens as a function of time of aging at 453 K.

larger than 1.6×10^{-2} .^[4] To obtain values of x'_{Cu} and x'_{Si} the following assumptions need to be made: (1) at the end temperature of effect A, no net precipitation is taking place; *i.e.*, the composition of the Al-rich matrix is given by the solid solubilities of copper and silicon; and (2) the solid solubilities of copper and silicon are independent; *i.e.*, the presence of silicon in solution does not alter the solubility of copper and *vice versa*. Then, the values of x'_{Cu} and x'_{Si} can simply be taken equal to the solid solubilities of copper and silicon in the Al-rich matrix as obtained from the respective binary phase diagrams^[2,20] at the end temperature of effect A (Table II). As silicon precipitates directly into the equilibrium phase, a single value for x'_{Si} results. Alternatively, two values are possible for copper: a value based on the equilibrium solid solubility corresponding to the precipitation of the θ phase and a value based on the metastable solid solubility corresponding to the precipitation of the θ' phase. Hence, the calculation in Appendix I was performed for the two types of copper precipitation indicated. Note that the difference between x_{Cu}^0 and x'_{Cu} is larger for the precipitation of the equilibrium θ phase than for the precipitation of the metastable θ' phase. In the case of the θ' -phase precipitation, application of Eq. [A11] for heating rates ≥ 40 K/min results in a zero or negative value of the amount of precipitating copper atoms. Apparently, no precipitation of copper as the θ' phase can then be expected. The result of the calculations are shown in Figure 9, where the calculated and the experimentally observed heat content of effect A is plotted as a function of the DSC heating rate. As follows from the binary phase diagrams, the values of x'_{Cu} and x'_{Si} increase with increasing end temperature, *i.e.*, increasing DSC heating rate. Hence, the amounts of silicon and copper atoms to precipitate decrease (Eqs. [A12] and [A13]), and thus, the heat content of effect A decreases also (Eq. [A15]). It can be seen from Figure 9 that the values for the combined silicon/ θ -phase precipitation are larger than for the combined silicon/ θ' -phase precipitation. This is due to the fact that (1) the heat of precipitation for the θ phase is larger than the heat of precipitation for the θ' phase (Appendix II), and (2) the number of copper atoms involved in θ -phase precipitation is larger than the number of copper atoms involved in θ' -phase precipitation (Eq. [A13]).

Table II. End Temperatures of Effect A, Binary Equilibrium and Metastable Solid Solubilities of Copper, and Solid Solubility of Silicon as a Function of Heating Rate^[2,20]

Heating Rate (K/min)	End Temp. of Effect A (K)	Binary Solid Solubility of		
		Copper		Silicon ($\times 10^2$)
		Equilibrium ($\times 10^2$)	Metastable ($\times 10^2$)	
0.5	525	0.10	0.46	0.018
2	570	0.18	0.61	0.044
5	595	0.24	0.71	0.069
20	640	0.41	1.08	0.147
40	675	0.60	1.58	0.235
80	705	0.83	>2	0.353

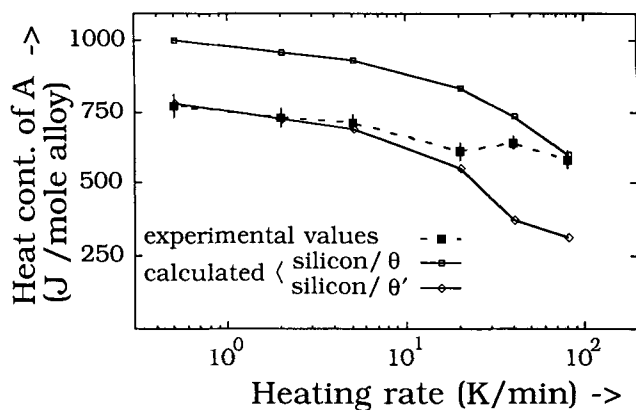


Fig. 9—The heat content of effect A for the SQ Al-1.3 at. pct Cu-19.1 at. pct Si alloy as a function of the DSC heating rate. The calculated values were obtained by applying Eqs. [A12] through [A15] and using solid solubility values from Table II.

From Figure 9, it is observed that the measured values of the heat content of effect A are always situated between the limits calculated for the cases of silicon/ θ' and of silicon/ θ precipitation. At the low heating rates (≤ 20 K/min), the experimental heat contents correspond very well with the calculated values for the case of the combined silicon/ θ' -phase precipitation. At these low heating rates, copper apparently precipitates mainly as the metastable θ' phase. For the high DSC heating rates (≥ 40 K/min), the experimental values correspond fairly well to the calculated values for the combined silicon/ θ -phase precipitation. Apparently, copper precipitation then proceeds mainly as equilibrium θ -phase precipitation.

2. Effect B

As silicon precipitates directly into its equilibrium phase, the only possible transformation giving rise to an exothermic heat effect after effect A is the transition from a state with the θ' phase into a state with the θ phase. A similar effect in the same temperature range was described by several authors.^[8,14,21-24] According to the findings of the previous section, the amount of θ' phase precipitated decreases with increasing DSC heating rate. Hence, interpreting effect B as due to the transition indicated, it is expected that the heat content of effect B decreases with increasing DSC heating rate. This is indeed observed (Table I). In the temperature range of effect B, a competition occurs between the transition of the state with copper precipitated as θ' phase to the state with copper precipitated as θ phase and the redissolution of copper. The two maxima of effect B observed at DSC heating rates 20 and 40 K/min may be related to this competition.

The amount of θ' phase precipitated, u , follows from Eqs. [A13] and [A4] and is given by

$$u = \frac{1 - x_{\text{Si}}^g}{1 - x_{\text{Si}}^0} \cdot \frac{x_{\text{Cu}}^0 - x'_{\text{Cu}}}{1 - (x'_{\text{Si}} + 3x'_{\text{Cu}})} \quad [2]$$

where x_{Si}^g represents the gross silicon content of the alloy. The amount of heat produced by the transition from the

state with copper precipitated as θ' phase into the state with copper precipitated as θ phase, Q_u , is now given by

$$Q_u = u \cdot \Delta H_{\theta'}^{\theta} \quad [3]$$

where $\Delta H_{\theta'}^{\theta}$ represents the difference between the heats of precipitation of the θ' phase and the θ phase and is taken equal to 10 kJ per mole copper (Appendix II).

In Table III, the theoretical estimates based on Eq. [3] are compared with the experimental values of the heat content of effect B. As can be seen, the theoretical predictions correspond very well to the experimentally observed values. These results also confirm that at low heating rates (≤ 20 K/min), copper precipitates mainly as θ' phase, whereas at high heating rates (≥ 40 K/min), the θ' -phase precipitation is nearly absent. As at the end temperatures related to the heating rates of 40 and 80 K/min x'_{Cu} is larger than x_{Cu}^0 , Eqs. [2] and [3] predict a zero value of Q_u for these heating rates. The nonzero values observed, however, indicate that even at these high heating rates, small amounts of θ' phase were still formed during the evolution of effect A.

3. GP-zone formation

Large changes in enthalpy have been determined to be indicative of GP-zone formation in Al-Cu-type alloys.^[25] In the SQ + NA specimens studied, an endothermic effect was observed just in advance of the main precipitation effect (Figure 5). The temperature range of this endothermic effect coincides with the temperature ranges for GP-zone dissolution in Al-Cu alloys observed by several authors.^[24,25] So, this endothermic effect is interpreted as due to GP-zone dissolution. Increasing the time of natural aging should increase the amount of GP zones formed, and the magnitude of this dissolution effect during DSC analysis should, therefore, accordingly increase. This behavior is indeed observed (Figure 6).

The heat effect of dissolution of GP zones formed at room temperature equals about 15 kJ per mole copper present as GP zones.^[25] Using this value, the mole fraction of copper present as GP zones in the SQ + NA specimens can be estimated. As can be deduced from Figure 6, the heat of dissolution of GP zones after 1000 hours of aging at room temperature is 17 J per mole alloy, which equals 21 J per mole Al-rich matrix

Table III. The Observed and Calculated Values of the Heat Content of Effect B as a Function of the Heating Rate*

Heating Rate (K/min)	Calculated Amount of θ' -Phase Precipitated (Eq. [2]) (Millimole)	Heat Content of Effect B (J per Mole Alloy)	
		Observed	Calculated
0.5	9.4	80 ± 30	94
2	8.2	60 ± 20	82
5	7.4	60 ± 20	74
20	4.3	41 ± 11	43
40	0	12 ± 5	0
80	0	8 ± 5	0

*At heating rates ≥ 40 K/min, no θ' -phase precipitation is expected; see Section IV-A-1.

(Eq. [A4]). Then, the fraction of copper atoms transformed into GP zones, $f_{\text{Cu}}^{\text{GP}}$, can readily be obtained:

$$f_{\text{Cu}}^{\text{GP}} = \frac{21}{15 \times 10^3 \cdot x_{\text{Cu}}^0} \approx 0.1$$

Literature data indicate that the formation of GP zones in conventional SQ Al-Cu alloys is finished within 200 hours of aging at ambient temperature.^[25,26,27] Baur and Gerold^[26] found that the fraction of copper atoms transformed into GP zones was 0.1 after 0.1 hours of aging at 301 K. Comparing this to the calculated fraction transformed of 0.1 after 1000 hours at room temperature in our alloy (see above) leads to an estimation of the relative formation rate of GP-zone formation: the GP-zone formation in the SQ Al-Cu-Si alloy is about 10^4 times slower than in the conventional SQ Al-Cu alloy. Here, the small difference in aging temperatures is neglected. This is justified, since this difference does not significantly influence the outcome of the estimation (the activation energy of GP-zone formation in SQ Al-Cu is about 0.6 eV^[19]).

The foregoing explains why nearly no traces of GP-zone dissolution could be detected during DSC measurements performed directly after solid quenching of the alloy studied: the lapse of time between solid quenching and the start of DSC experiments was far too small to allow the formation of an appreciable amount of GP zones. The suppression of GP-zone formation was also observed in quenched MMCs.^[6,7,8] Comparing DSC runs of rapidly cooled and subsequently aged samples of an Al-Cu alloy with reinforcement (20 wt pct $\text{Al}_2\text{O}_3/\text{SiO}_2$ fibers) and without reinforcement, Abis and Donzelli^[8] observed that the reinforced alloy showed no trace of GP-zone dissolution, while the unreinforced alloy did show significant GP-zone dissolution. Papazian^[7] also observed reduced GP-zone dissolution enthalpies in a quenched fiber-reinforced Al-Cu alloy (2219) as compared to the corresponding unreinforced alloy. Also, in a fiber-reinforced Al-Mg-Si alloy (6061), a suppression of GP-zone formation has been observed.^[6] The reduced GP-zone formation was explained by the annihilation of excess vacancies by misfit dislocations, which were created in the reinforced alloys on cooling after thermal treatment by virtue of the large difference in thermal expansion coefficients of matrix and reinforcement.^[7,8] As in the Al-Cu-Si alloy studied the silicon particles and the Al-rich matrix also have a large difference in thermal expansion coefficients, misfit will occur on cooling or quenching between the matrix and the silicon particles. Analogous to the case of the quenched particle-reinforced MMCs, the suppression of GP-zone formation observed for the SQ Al-Cu-Si alloy can be related to that misfit (for a more detailed discussion, see Reference 13).

4. Kinetics of precipitation

Consider the state variable, β , defined by

$$\beta(t) = \int_0^t k dt = \int_0^t \left[k_0 \exp\left(\frac{-E_A}{k_B T}\right) \right] dt \quad [4]$$

where E_A is an effective activation energy describing the overall precipitation process and t , k_0 , k_B , and T denote,

respectively, time of aging, a pre-exponential factor, Boltzmann's constant, and the absolute temperature. For nonisothermal annealing with a constant heating rate (*i.e.*, the case of DSC experiments), it was recently shown^[28] that the following relationship between the temperature for a fixed stage of transformation, T_f , and the heating rate, Φ , holds:

$$\ln \frac{T_f^2}{\Phi} = \frac{E_A}{k_B T_f} + \beta_f \quad [5]$$

In deriving Eq. [5], it was assumed that β could be considered as a state variable, fully determining the extent of the transformation process involved. It can be shown that the maximal transformation rate corresponds to an approximately constant stage of transformation and that, for DSC experiments, the temperature of maximal transformation rate is given by the peak temperature.^[28,29] In the case of the precipitation in an SQ Al-Cu-Si alloy, where the heat evolution observed during a DSC experiment results from the synchronically preceding silicon and copper precipitation (Section IV-A-1) for the heating rates ≤ 20 K/min, it appeared that the heat evolution stems solely from the combined silicon/ θ' -phase precipitation, whereas at 40 and 80 K/min, the θ -phase precipitation must also be taken into account. Thus, it was decided to obtain an effective value for the activation energy only for heating rates ≤ 20 K/min. From the slope of straight lines through the data points of the plots of $\ln(T_f^2/\Phi)$ vs $1/T_f$, at certain transformation stages, values of effective activation energies were obtained. Four transformation stages were chosen: (1) at the peak temperature, (2) at 10 pct, (3) at 50 pct, and (4) at 90 pct of the total heat development during effect A. The values obtained for the four different stages of combined precipitation did not differ significantly. The average value of the effective activation energy was calculated to be

$$E_A = 1.00 \pm 0.07 \text{ eV}$$

This value corresponds fairly well to the value of the activation energy of silicon precipitation in SQ ribbons of an Al-Si alloy,^[11] where an excess of vacancies could be expected. The values for the activation energy for self-diffusion in aluminum and for both silicon and copper diffusion in aluminum (all about 1.3 eV^[19]) are larger than the value obtained for E_A . As both silicon and copper atoms are substitutionally dissolved in the Al-matrix and both silicon and copper precipitation can only proceed *via* a vacancy mechanism, the low activation energy of precipitation in the SQ Al-Cu-Si alloy suggests that the precipitation kinetics are enhanced by excess vacancies. This result may be somewhat surprising, in view of the presence of a large amount of finely dispersed silicon particles and, specifically, the large amount of interfaces that can act as vacancy sinks. However, silicon occupies a much larger volume when precipitated than when dissolved in the Al-rich matrix.^[12] The volume misfit between silicon particles just precipitated and the surrounding Al-rich matrix can be accommodated by excess vacancies,^[30] which may, according to Russell,^[31] precipitate near the precipitate/matrix interface, thus relieving transformation strains. Thus, the newly formed

interfaces can also act as temporary sources of vacancies. Further, on quenching, excess vacancies can condense into vacancy loops, which on aging also may act as temporary sources of vacancies.^[32,33] Also, the suppression of GP-zone formation observed for the SQ Al-Cu-Si alloy (Section IV-A-3) can contribute, at least partly, to the retaining of excess vacancies.^[13]

The temperature region of silicon precipitation in SQ Al-Si alloys during heating with a heating rate of 5 K/min is located at about 460 to 560 K (this follows from Reference 1). This corresponds fairly well to the temperature range of effect A (the combined silicon and copper precipitation) in our alloy. The precipitation of copper in an SQ Al-Cu, however, proceeds in a higher temperature range (520 to 630 K at 5 K/min; see Reference 13). Also, given the good correspondence between the effective activation energy for precipitation and the activation energy for silicon precipitation in SQ Al-Si ribbons, these results suggest that the precipitation is lead by a vacancy-enhanced precipitation of silicon atoms dragging the copper atoms.

B. Precipitation Effects Directly after Extrusion

The absence of effects A and B in the DSC curves of the AE specimen (Figure 7) indicates that during preheating for 20 minutes and subsequent extrusion, precipitation had already proceeded to a large extent. However, the hardness increase as observed on aging of the AE specimen (Figure 8) can only be interpreted as due to precipitation of a copper-containing phase, as silicon precipitation does not cause a significant hardness increase.^[19]

At the preheating and extrusion temperature, the equilibrium and the metastable solid solubilities of copper are 0.5×10^{-2} and 1.3×10^{-2} , respectively.^[2] It is unlikely that during extrusion, θ' phase was formed, since in that case, the AE specimens should possess an Al-rich matrix with a dissolved copper fraction of at least 1.3×10^{-2} (cooling after extrusion was relatively fast: 10 minutes in air followed by a water quench). However, DSC analysis shows that no such large supersaturation in AE examples exists, since no exothermic precipitation effect is observed. Hence, it can safely be assumed that preheating and extrusion resulted in precipitation of the equilibrium θ phase, thus leaving an Al-rich matrix with a copper fraction of about 0.5×10^{-2} after cooling.

Thus, the Al-rich matrix in the SQ specimen possessed a higher copper fraction than the Al-rich matrix in the AE specimens. As GP-zone formation in the SQ specimens was suppressed (Section IV-A-3), GP-zone formation in the AE specimens cannot be expected. This is confirmed: no traces of GP-zone dissolution are observed in the DSC curves for the AE and AE + A specimens (Figure 7). The only copper precipitate apart from GP zones that can cause the observed hardness increase upon aging is the semicoherent θ' -phase precipitate.^[19] So, it is concluded that in the AE specimens, precipitation involves the formation of θ' phase. Increasing the time of aging at 453 K increases the amount of semicoherent θ' phase formed, and this causes an initial increase of the hardness as a function of aging time. Later,

beyond 28 hours of aging at 453 K, the hardness decreases (Figure 8). This may be related to coarsening of the θ' phase.^[14] The endothermic effects observed in Figure 7 for the AE + A specimens can only be caused by a dissolution effect starting at lower temperatures than the temperatures of the equilibrium-phase dissolution during the rescans (Section III). Indeed, the θ' -phase dissolution starts at lower temperatures than the θ -phase dissolution.^[2] Therefore, the increasing magnitude of the endothermic effect, as observed in Figure 7, is interpreted as caused by the dissolution of increasing amounts of θ' phase. Apparently, the formation of θ' phase continues up to 192 hours of aging at 453 K.

V. CONCLUSIONS

1. The heat content of the combined precipitation peak in the SQ Al-Cu-Si alloy (effect A) can quantitatively be described in terms of the heats of precipitation of both alloying elements and in terms of solid solubilities of the constituting binary alloys.
2. The heat content of the exothermic effect due to the replacement of the θ' phase by the θ phase, effect B in the SQ Al-Cu-Si alloy, agrees with the difference in heat of precipitation of these phases.
3. During nonisothermal annealing with constant heating rate of the SQ Al-Cu-Si alloy, silicon and copper atoms precipitate simultaneously: at low heating rates (≤ 20 K/min), as silicon and θ' phase, and at high heating rates (≥ 40 K/min), mainly as silicon and θ phase.
4. The temperature range of the combined precipitation in the SQ Al-Cu-Si alloy corresponds to that of the precipitation in the SQ Al-Si alloy but is much lower than that of the precipitation in the SQ Al-Cu alloy.
5. The effective activation energy for the combined precipitation in the SQ Al-Cu-Si alloy is much lower than the activation energy for self-diffusion and for copper and silicon diffusion in aluminum, denoting a vacancy-enhanced precipitation mechanism.
6. Guinier-Preston-zone formation in the SQ Al-Cu-Si alloy is approximately 10^4 times slower than in SQ Al-Cu alloys.
7. The matrix of the AE Al-Cu-Si alloy is supersaturated with copper; aging at 453 K after extrusion yields a hardness increase due to the formation of θ' -phase precipitates.

APPENDIX I

Consider one mole of the ternary Al-Cu-Si alloy with gross silicon and copper contents, x_{Si}^g mole and x_{Cu}^g mole, respectively. At the start of precipitation, silicon is partly dissolved in the Al-rich matrix, and copper is wholly dissolved in the Al-rich matrix. It is assumed that no aluminum is dissolved in silicon. Let the heats of precipitation per mole precipitating silicon or copper be ΔH_{Si} and ΔH_{Cu} , respectively. Let ΔH_{Si} and ΔH_{Cu} for the ternary alloy be equal to the values for the respective binary alloy systems. Denote Q as the heat evolved during precipitation per mole alloy and Q_M as the heat evolved

during precipitation per mole matrix. The amount of aluminum present is given by

$$1 - (x_{\text{Si}}^g + x_{\text{Cu}}^g)$$

If the amount of silicon dissolved in the Al-rich matrix is given by s moles, then the mole fraction silicon dissolved in the Al-rich matrix at the start of precipitation, x_{Si}^0 , is given by^[1,34]

$$x_{\text{Si}}^0 = \frac{s}{1 - (x_{\text{Si}}^g + x_{\text{Cu}}^g) + s + x_{\text{Cu}}^g} = \frac{s}{1 - x_{\text{Si}}^g + s} \quad [\text{A1}]$$

The mole fraction copper of the Al-rich matrix at the start of precipitation, x_{Cu}^0 , is given by

$$x_{\text{Cu}}^0 = \frac{x_{\text{Cu}}^g}{1 - x_{\text{Si}}^g + s} \quad [\text{A2}]$$

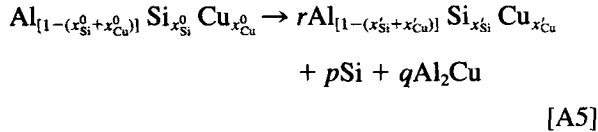
From Eq. [A1] follows

$$s = \frac{1 - x_{\text{Si}}^g}{1 - x_{\text{Si}}^0} x_{\text{Si}}^0 \quad [\text{A3}]$$

and the amount of Al-rich matrix (number of moles) is

$$1 - x_{\text{Si}}^g + s = \frac{1 - x_{\text{Si}}^g}{1 - x_{\text{Si}}^0} \quad [\text{A4}]$$

After a certain precipitation time, the mole fractions silicon and copper of the Al-rich matrix are given by x'_{Si} and x'_{Cu} , respectively. The precipitation reaction can be represented by



where r , p , and q represent the amounts (number of moles) of Al-rich phase, silicon phase, and Al_2Cu phase (θ or θ'), respectively. It is assumed that the θ phase and the θ' phase have the same chemical composition: Al_2Cu , and that silicon precipitates as pure silicon.

Conservation of mass requires for aluminum:

$$1 - (x_{\text{Si}}^0 + x_{\text{Cu}}^0) = r[1 - (x'_{\text{Si}} + x'_{\text{Cu}})] + 2q \quad [\text{A6}]$$

for silicon:

$$x_{\text{Si}}^0 = rx'_{\text{Si}} + p \quad [\text{A7}]$$

for copper:

$$x_{\text{Cu}}^0 = rx'_{\text{Cu}} + q \quad [\text{A8}]$$

From Eqs. [A6] through [A8] follows

$$p = \frac{x_{\text{Si}}^0 - x'_{\text{Si}} - 3(x_{\text{Si}}^0 x'_{\text{Cu}} - x'_{\text{Si}} x_{\text{Cu}}^0)}{1 - (x'_{\text{Si}} + 3x'_{\text{Cu}})} \quad [\text{A9}]$$

$$q = \frac{x_{\text{Cu}}^0 - x'_{\text{Cu}} - (x'_{\text{Si}} x_{\text{Cu}}^0 - x_{\text{Si}}^0 x'_{\text{Cu}})}{1 - (x'_{\text{Si}} + 3x'_{\text{Cu}})} \quad [\text{A10}]$$

$$r = \frac{1 - (x_{\text{Si}}^0 + 3x_{\text{Cu}}^0)}{1 - (x'_{\text{Si}} + 3x'_{\text{Cu}})} \quad [\text{A11}]$$

In view of the maximal values possible for the con-

centrations occurring in these formulas (Table II), the product terms in Eqs. [A9] and [A10] can generally be neglected; this gives

$$p = \frac{x_{\text{Si}}^0 - x'_{\text{Si}}}{1 - (x'_{\text{Si}} + 3x'_{\text{Cu}})} \quad [\text{A12}]$$

$$q = \frac{x_{\text{Cu}}^0 - x'_{\text{Cu}}}{1 - (x'_{\text{Si}} + 3x'_{\text{Cu}})} \quad [\text{A13}]$$

The value of Q_M is now given by

$$Q_M = p\Delta H_{\text{Si}} + q\Delta H_{\text{Cu}} \quad [\text{A14}]$$

and the value of Q by

$$Q = Q_M \frac{1 - x_{\text{Si}}^g}{1 - x_{\text{Si}}^0} \quad [\text{A15}]$$

APPENDIX II

The value of ΔH_{Si} can be directly obtained from literature data:^[1] $\Delta H_{\text{Si}} = 54$ kJ/mole. Following the reasoning of Van Rooijen *et al.*,^[11] values for ΔH_{Cu} can be obtained from literature data on the solid solubility of copper in the Al-rich matrix. In the case of the precipitation of copper as the equilibrium θ phase, the heat of precipitation, $\Delta H_{\text{Cu}}^\theta$, is obtained from the slope of the straight line through the data points of the plot of the logarithm of the equilibrium solid solubility vs the reciprocal temperature. Solid solubility data were taken from References 35 through 38, also cited by Murray.^[2] The slope of the resultant line, and thus, $\Delta H_{\text{Cu}}^\theta$, was determined to be 44 ± 1 kJ/mole. Nakamura *et al.*^[39] obtained a corresponding value based on independently determined solid solubility data. The heat of precipitation of copper as the metastable θ' phase, $\Delta H_{\text{Cu}}^{\theta'}$, was obtained analogously (data from the metastable solvus were taken from References 23, 38, and 40, as cited by Murray^[2]), yielding $\Delta H_{\text{Cu}}^{\theta'} = 34 \pm 4$ kJ/mole. This value is intermediate between the values reported for the heat of formation of GP II zones and for the heat of formation of the equilibrium θ phase.^[39] This is in accordance with thermodynamics, which predicts an increasing stability of the precipitates successively formed during the full precipitation sequence. Now, the heat of the transition from the state with copper precipitated as θ' phase to the state with copper precipitated as θ phase is given by

$$\Delta H_{\theta'}^\theta = \Delta H_{\text{Cu}}^\theta - \Delta H_{\text{Cu}}^{\theta'} = 10 \pm 5 \text{ kJ/mole}$$

ACKNOWLEDGMENTS

The authors are indebted to Mr. P. de Ruiter and Mr. H. Kleinjan for providing the melt-spun alloy, to Dr. Inz. J. Duszcyk and Zhou Jie, M.Sc., for performing the extrusion, to Mr. P.F. Colijn for assistance with optical microscopy, and to Mr. P.J. van der Schaaf for overall practical assistance. Stimulating discussions with Professor B.M. Korevaar, who critically read the manuscript, and Dr. W.H. Kool are gratefully acknowledged. The financial support of the Foundation for Fundamental Research of Matter and for Technological Sciences (FOM/STW) is gratefully acknowledged.

REFERENCES

1. M. van Rooyen and E.J. Mittemeijer: *Metall. Trans. A*, 1989, vol. 20A, pp. 1207-14.
2. J.L. Murray: *Int. Met. Rev.*, 1985, vol. 30, pp. 211-33.
3. V. Gerold: *Scripta Metall.*, 1988, vol. 22, pp. 927-32 and subsequent papers in *Viewpoint Set*, pp. 927-62.
4. H.W.L. Phillips: *Annotated Equilibrium Diagrams of Some Aluminum Alloy Systems*, Institute of Metals Monograph and Report Series 25, The Institute of Metals, London, 1959.
5. C.M. Friend, R. Young, and I. Horsfall: *Proc. 3rd European Conf. on Composite Materials*, Bordeaux, France, March 20-23, 1989, A.R. Bunsell, ed., Elsevier Applied Science, London, 1989, pp. 227-32.
6. C.M. Friend and S.D. Luxton: *J. Mater. Sci.*, 1988, vol. 23, pp. 3173-80.
7. J.M. Papazian: *Metall. Trans. A*, 1988, vol. 19A, pp. 2945-53.
8. S. Abis and G. Donzelli: *J. Mater. Sci. Lett.*, 1988, vol. 7, pp. 51-52.
9. T. Christman and S. Suresh: *Acta Metall.*, 1988, vol. 36, pp. 1691-1704.
10. T.G. Nieh and R.F. Karlak: *Scripta Metall.*, 1984, vol. 18, pp. 25-28.
11. M. van Rooyen, P.F. Colijn, Th. H. de Keijser, and E.J. Mittemeijer: *J. Mater. Sci.*, 1986, vol. 21, pp. 2373-84.
12. E.J. Mittemeijer, P. van Mourik, and Th.H. de Keijser: *Phil. Mag. A*, 1981, vol. 43, pp. 1157-64.
13. M.J. Starink and P. van Mourik: *Proc. Int. Conf. on Advanced Aluminium and Magnesium Alloys*, Amsterdam, The Netherlands, June 20-22, 1990, in press.
14. K. Hirano and H. Iwasaki: *Trans. Jpn. Inst. Met.*, 1964, vol. 5, pp. 162-70.
15. M. van Rooyen, J.A. van der Hoeven, L. Katgerman, P. van Mourik, Th.H. de Keijser, and E.J. Mittemeijer: *Proc. PM Aerospace Mater. Conf.*, Metal Powder Report, ed., Bern, Switzerland, Nov. 12-14, 1984.
16. *Metals Reference Book*, 5th ed., C.J. Smithells, ed., Butterworth's, London, 1976.
17. *Metals Reference Book*, 5th ed., C.J. Smithells, ed., Butterworth's, London, 1976, p. 221.
18. J.M. Papazian: *Metall. Trans. A*, 1981, vol. 12A, pp. 269-80.
19. L.F. Mondolfo: *Aluminium Alloys: Structure and Properties*, Butterworth's, London, 1976.
20. J.L. Murray and A.J. McAlister: *Bull. Alloy Phase Diagrams*, 1984, vol. 5, pp. 74-84.
21. I.L. Polmear and H.K. Hardy: *J. Inst. Met.*, 1954, vol. 83, pp. 393-94.
22. A.M. Zahra, C.Y. Zahra, and M. Laffite: *Scripta Metall.*, 1975, vol. 9, pp. 879-86.
23. A.M. Zahra, M. Laffite, P. Vigier, and M. Wintenberger: *C.R. Acad. Sci.*, 1973, vol. 277, pp. 923-25.
24. C. Garcia-Cordovilla and E. Louis: *Metall. Trans. A*, 1984, vol. 15A, pp. 389-91.
25. A.M. Zahra, M. Laffite, P. Vigier, and M. Wintenberger: *Mem. Sci. Rev. Metall.*, 1977, vol. 74, pp. 561-67.
26. R. Baur and V. Gerold: *Z. Metallkd.*, 1966, vol. 57, pp. 181-86.
27. C. Chiou, H. Herman, and M.E. Fine: *Trans. AIME*, 1960, vol. 218, pp. 299-307.
28. E.J. Mittemeijer, L. Cheng, P.J. van der Schaaf, C.M. Brakman, and B.M. Korevaar: *Metall. Trans. A*, 1988, vol. 19A, pp. 925-32.
29. E.J. Mittemeijer, A. van Gent, and P.J. van der Schaaf: *Metall. Trans. A*, 1986, vol. 17A, pp. 1441-45.
30. D. Segers, P. van Mourik, M.H. van Wijngaarden, and B.M. Rao: *Phys. Status Solidi*, 1984, vol. 81, pp. 209-16.
31. K.C. Russell: *Scripta Metall.*, 1970, vol. 3, pp. 313-16.
32. E. Ozawa and H. Kimura: *Acta Metall.*, 1970, vol. 18, pp. 995-1004.
33. E. Ozawa and H. Kimura: *Mater. Sci. Eng.*, 1971, vol. 8, pp. 327-35.
34. P. van Mourik, E.J. Mittemeijer, and Th.H. de Keijser: *J. Mater. Sci.*, 1983, vol. 18, pp. 2706-20.
35. A. Phillips and R.M. Brick: *J. Franklin Inst.*, 1933, vol. 215, pp. 557-77.
36. R.H. Brown, W.L. Fink, and M.S. Hunter: *Trans. AIME*, 1941, vol. 143, pp. 117-23.
37. E.C. Ellwood and J.M. Silcock: *J. Inst. Met.*, 1948, vol. 74, pp. 457-67.
38. G. Borelius, J. Anderson, and K. Gullberg: *Ing. Vetenskaps Akad. Handl.*, 1943, vol. 169, pp. 5-27.
39. F. Nakamura, F. Furukawa, M. Yanai, and J. Takamura: *Phil. Mag. A*, 1986, vol. 54, pp. 67-78.
40. K. Matsuyama: *Kinzoku-no Kenkyu*, 1934, vol. 11, pp. 461-90.